Two-Dimensional Fiber-Optic Control of a True Time-Steered Array Transmitter

Michael Y. Frankel, Paul J. Matthews, and Ronald D. Esman, *Senior Member, IEEE*

Abstract— **We report a first demonstration of a fiber-optic beamformer for independent two-dimensional (2-D) true time-delay steering of a transmitter array. The fiber-optic beamformer is based on a simple dispersive prism optical delay approach, with separate azimuth and elevation control stages. The azimuth dispersive prism stage includes an amount of dispersion in each link proportional to the corresponding column position in the array. The microwave signals, properly time-delayed for azimuth steering, are amplified and serve as inputs to identical dispersive prisms feeding the elements in each column. The elevation dispersive prism stages include an amount of dispersion in each link proportional to the corresponding row position in the array. Each time-delayed microwave signal feeds a single flared-notch element in a 4 × 4 array. The 2-D array pattern measurements in an anechoic chamber clearly demonstrate independent ±30° azimuth and ±30° elevation steering. There is no observed squint over the microwave-component determined bandwidth of 6–18 GHz.**

I. Introduction

PHOTONIC control of phased-array antennas has seen active recent development [1]. The development efforts are mostly driven by the expected benefits over conventional all-electronic phased-array antenna control methods in the areas of size and weight reduction, interference immunity, remoting capability, etc. In addition, photonics has held out a promise of being an enabling technology for true time-delay beam steering, which permits wide instantaneous bandwidths and squint free operation. A variety of photonic techniques have been proposed for obtaining true time-delay capability. Among others, these include electronically-selected optical delay lines [2], switched optical delay lines [3], [4], [5], optimized schemes combining both optical and electronic time-delay switching [6], schemes based on optically-coherent control of arrays [7], acoustooptically based delay lines [8], fiber Bragg grating-based delay lines [9], and schemes based on fiber-optic dispersive delay lines [10], [11]. However, most of these techniques have not progressed beyond conceptual laboratory demonstrations, as they are hampered by the demands for precisely matched optical elements, excessive power losses, instability, or specialized component development. The exceptions have been the switched delay line techniques developed by [2] and [6] for MHz through 3 GHz frequency ranges, and a dispersive delay line technique developed by ourselves for under 2 to over 18 GHz frequency ranges. Recently, we demonstrated a true time-delay fiber-optic control of an eight-element one-dimensional transmitter array which exhibited squint-free 500 azimuth steering over a 2 to 18 GHz frequency range [11].

Here, we demonstrate what we believe is the first complete two-dimensional (2-D) true time-delay control of an ultrawideband transmitter array. The system exhibits an unprecedented combination of independent ±30° azimuth and ±30° elevation steering over a microwave component-limited bandwidth of 6 to 18 GHz. Thus, the technique has overcome the problems discussed above and shows the capability to be transitioned to real-world ultrawideband array transmitters.

Manuscript received March 29, 1996. This work was supported by the Office of Naval Research.

The authors are with Optical Sciences Division, Naval Research Laboratory, CODE 5672, Washington, DC 20375-5338.

Publisher Item Identifier S 0018-9480(96)08575-4.

II. System Configuration

The total fiber-optic beamformer system is shown schematically in Fig. 1. The optical sources for both azimuth and elevation steering control are fiber-optic Iota-lasers [12] with single-polarization output which is continuously tunable over a range of >50 nm around 1540 nm. The system functionality is described as follows. An electrooptic Mach–Zehnder modulator (MZM) in the azimuth fiber-optic prism stage is driven by the system microwave input signal. The MZM modulates the amplified laser output and then the modulated optical carrier is fed to a 4-channel fiber-optic dispersive prism. The prism provides dispersion in each link which is proportional to the position of a corresponding column of antenna elements within the array. Thus, tuning the wavelength of the laser (λ_{az}) changes the delay of the microwave signals demodulated by the individual link p-i-n photodiodes (PD) and produces azimuth steering.

The microwave signals, appropriately time-delayed for azimuth control, are in turn amplified by a set of matched amplifiers and fed as inputs to a bank of nominally-identical MZM's. The optical carrier from another Iota laser is corporately distributed to the MZM's and fed to a set of nominally-identical fiber-optic dispersive prisms providing dispersion in each link proportional to the position of the corresponding row of antenna elements within the array. Thus, tuning the wavelength of the second laser (λ_{el}) imparts additional delays onto the microwave signals and effects elevation steering.

A nominal unit length of $\ell_{hd} = 200$ m of high-dispersion (HD) fiber from Corning ($D_{hd} \sim -88$ ps/nm ·km) was used in the azimuth-controlling prism. Thus, the consecutive links had 0, 200, 400, and 600 m of HD fiber respectively. The overall link lengths were equalized with dispersion-shifted (DS) fiber to produce equal interlink delay at $\lambda_{az} = 1540$ nm. A nominal unit length of $\ell_{hd} = 50$ m of HD fiber was used in the four

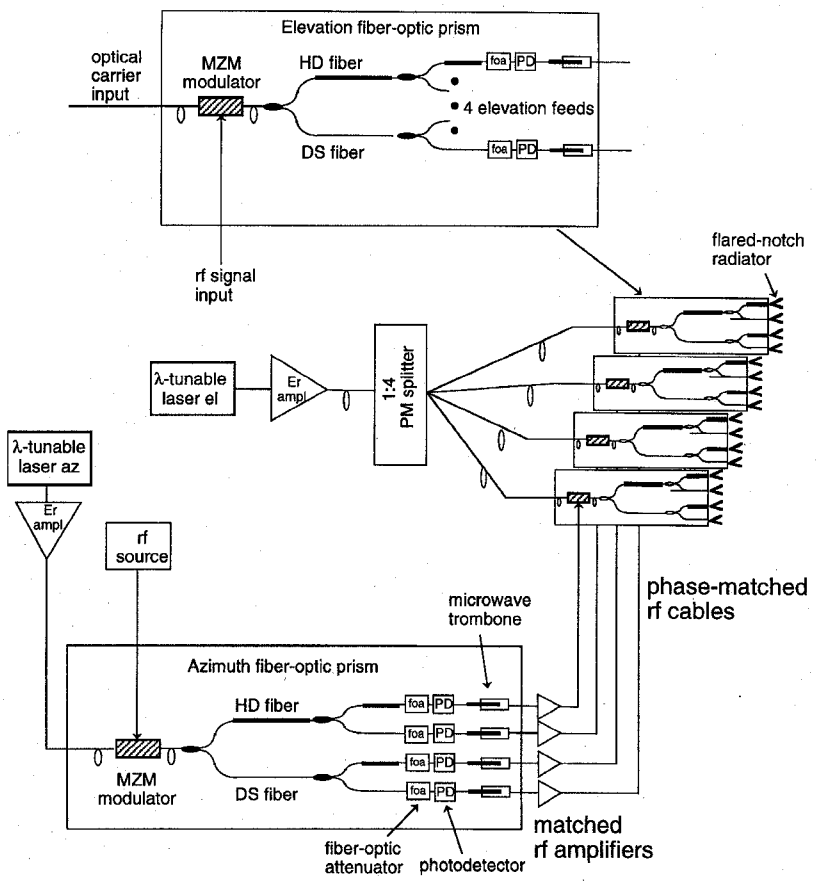

Fig. 1. Fiber-optic beamformer schematic diagram.

identical elevation-controlling prisms, with the overall delays equalized with DS fiber at $\lambda_{el} = 1540.5$ nm. The required precision of HD and DS fiber trimming for proper system performance has been discussed previously, and does not pose a significant problem [11].

The required wavelength detuning $\Delta\lambda$ for a given optical steering angle can be computed as

$$\Delta\lambda = \frac{d_e}{c \cdot D_{hd} \cdot l_{hd}} \cdot \sin(\Theta_o) \tag{1}$$

where d_e is the element spacing, c is the speed of light in air, and Θ_o is the required steering angle.

Each fiber-optic link also included a fiber-optic attenuator (FOA) for microwave frequency-independent interlink gain equalization and a microwave trombone for small time-delay error trimming during the system calibration procedure. Furthermore, microwave isolators were used after all photodiodes to reduce the system response rf ripple due to their high-output impedance.

III. Beamformer Benchtop Characterization

After assembly and packaging and prior to anechoic chamber tests, the fiber-optic beamformer system was calibrated and characterized on the benchtop. Several parameters were evaluated to ascertain that the system functioned as designed. First, the HD fiber dispersion was verified to be uniform along the length of the source spool to within the measurement resolution of ± 1 ps/nm·km. The fiber dispersion variation created problems in the previous tests [11], but was not a concern in these tests due to improved fiber uniformity characteristics.

Second, the four fiber-optic link responses of the azimuth prism were measured as shown in Fig. 2. These were verified to be consistent with the MZM half-wave voltage (V_π) of ~15 V, the average PD photocurrent of ~0.6 mA, and the microwave losses associated with additional microwave components (bias Tee, trombone, isolator, connectors, etc.). Furthermore, ~39-dB gain, ~3-dB noise figure microwave amplifiers were incorporated into each azimuth prism fiber-optic link to partially compensate for the link insertion losses. The amplifiers were from a set matched to ± 1 dB in gain and $\pm 10°$ in phase across the complete 6 to 18 GHz frequency band. Indeed, it was this variation that defined the interlink gain and phase tracking inaccuracies at this stage of the system. The strong roll-off in the link gain with increasing frequency (see Fig. 2) is primarily due to the combined effect of the MZM and PD responses. The response resonances observed at 11.5 GHz, 16 GHz, and 16.8 GHz were traced to the MZM. The MZM's used in this system were pre-production devices, and we believe that these resonances can be easily eliminated in the improved production versions. Alternately, MZM's from other suppliers can also be used.

The system noise floor at this stage was verified to be determined by the thermal noise at the input of the microwave amplifiers, with the contribution of laser and Er amplifier noise being negligible.

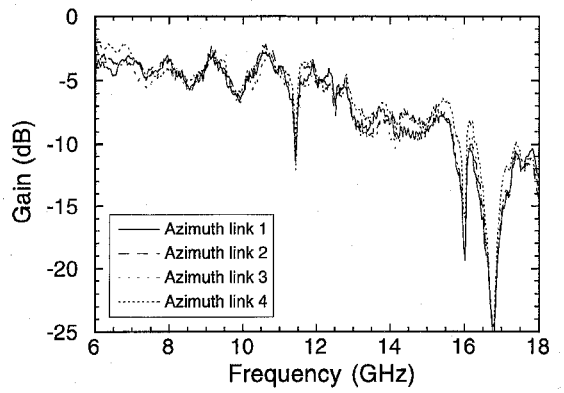

Fig. 2. Frequency response of the four links of the azimuth fiber-optic prism, as measured at the input of the elevation prism MZM's.

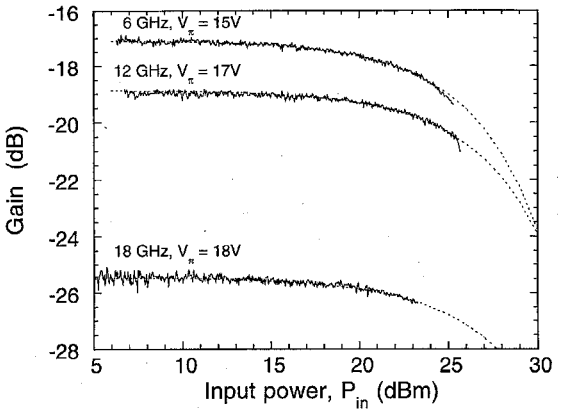

Fig. 3. Measured (solid) and calculated (dashed) gain saturation characteristics of the azimuth prism MZM at 6, 12, and 18 GHz. The fitted half-wave voltages are indicated on the plot.

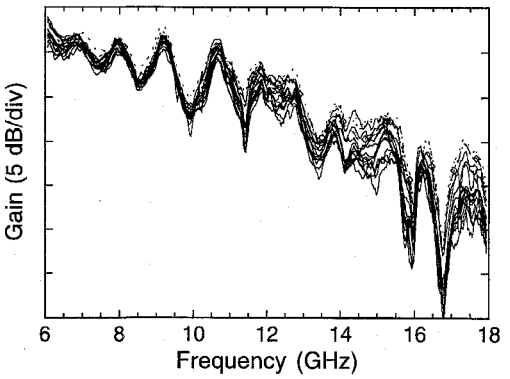

Fig. 4. Frequency-domain amplitude tracking of the 16 feeds to the array elements.

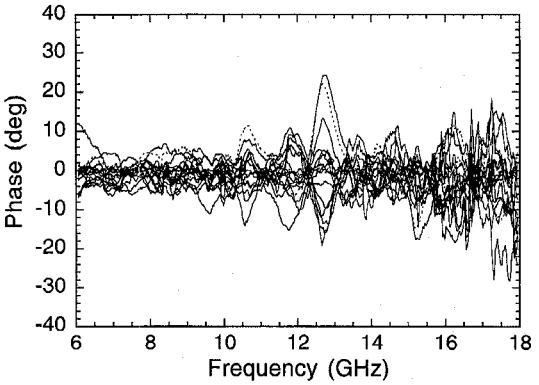

Fig. 5. Frequency-domain phase tracking of the 16 feeds to the array elements, normalized to element in row one, column one.

The system dynamic range was limited by the saturation of the azimuth stage MZM, since all PD's and microwave amplifiers were operated well below their saturation points. Fig. 3 shows the measured and calculated MZM gain saturation characteristics at three frequencies. The calculated characteristics [13] used the frequency-dependent voltage V_π as the fitting parameter, and the fitted values are consistent with the MZM response roll-off and fiber-optic link loss measurements.

As the final diagnostic of the system microwave performance characteristics, the amplitude and phase tracking of the microwave signals feeding the 16 antenna elements were measured. The system bandwidth characteristics require that the signals feeding individual antenna elements track in both amplitude and phase across the complete 6 to 18 GHz frequency range simultaneously. Fig. 4 shows the amplitude tracking of the 16 microwave signals feeding the individual antenna radiating elements across the 6 to 18 GHz frequency range. Fig. 5 shows the phase tracking of the same 16 signals normalized to one of them to remove the large phase slope due to the signal propagation delay through the fiber-optic prisms. The observed RMS variation of ± 1 dB and $\pm 5°$ at low and intermediate frequencies is due to the individual microwave component variation from link to link. The increased RMS variation of ± 2.5 dB and $\pm 10°$ at high frequencies is determined by the differences among the microwave amplifiers and the MZM's used to drive each elevation prism, with these errors being common to all elements in a single column.

The array is optically steered by tuning the wavelength of the azimuth and elevation laser sources. Thus, in addition to the frequency-dependent errors that cannot be easily corrected due to the broad-band nature of the system, there are additional wavelength-dependent errors that may come into play. In our system, the wavelength dependence of the characteristics of the optical fibers, MZM's and PD's was small. The dominant error factor was the wavelength dependence of the fiber-optic couplers, which were standard types specified to ± 0.3-dB coupling ratio tolerance. Fig. 6 shows the measured wavelength dependence of a 10 GHz microwave signal amplitude of the four azimuth prism links referenced to the first one. The observed wavelength dependence is less than ± 0.4 dB over the 1525 to 1548 nm range, but increases considerably above 1550 nm. We have therefore selected a wavelength of 1540 nm for the azimuth prism and 1540.5 nm for the elevation prisms as the center wavelength to maintain high optical power while minimizing the signal wavelength dependence during optical array steering.

It should be noted that real arrays are expected to incorporate electronic attenuators making it possible to dynamically

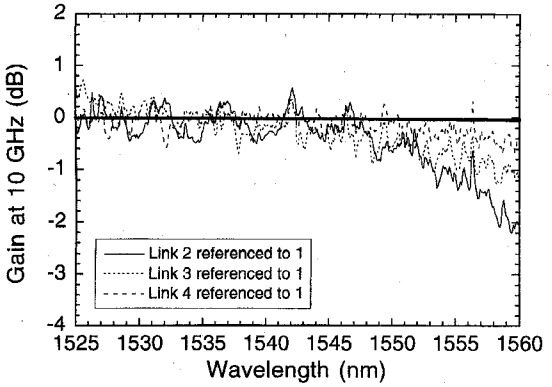

Fig. 6. Wavelength dependence of the three azimuth prism fiber-optic links normalized to the first one.

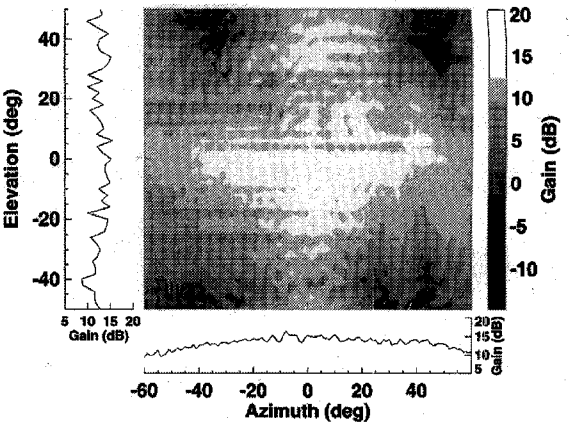

Fig. 7. An intensity plot and the cardinal azimuth and elevation axis cuts for the single-element pattern at 12.2 GHz.

compensate for the residual wavelength dependence during array steering.

IV. Anechoic Chamber Characterization

The antenna with a fiber-optic beamformer was tested in a compact radar range using a network analyzer to drive the system and to detect the received signal. Both the azimuth and elevation control lasers and the system input MZM were placed in the operator control room. The remaining components of the fiber-optic beamformer were mounted inside an aluminum box and were positioned inside the anechoic chamber. The beamformer was controlled solely through one single-mode fiber feeding the azimuth dispersive prism and one polarization-maintaining fiber feeding the four elevation dispersive prisms.

The 8×32 array antenna elements were flared-notch elements suitable for operation over the 6 to 18 GHz band, and were arranged on a rectangular grid [14]. The 4×4 actively driven elements were separated by 3.7 cm and 0.93 cm in the azimuth and elevation directions, respectively. The undriven elements were terminated into 50 Ω.

The high microwave insertion loss of the elevation-control fiber-optic prisms created a problem during these tests. There was a large coherent background radiation picked up by the receiver due to the microwave signal leakage from the amplifiers feeding the elevation MZM's. This background radiation was only 10–20 dB below the actual radiated signal level and introduced a ripple on the antenna patterns and corrupted the measurement of the pattern nulls. Fortunately, this background radiation preceded the actual one in time by the signal propagation delay through the elevation prism. Therefore, we used the network analyzer time windowing facility to numerically remove this signal component from the measurements. An improved system design would incorporate better amplifier shielding and additional microwave amplifiers feeding the radiating elements to boost the desired radiated signal level.

Fig. 7 shows an intensity plot and the cardinal azimuth and elevation axis cuts for the single element patterns at 12.2 GHz. The element patterns give an indication of how well the array may be expected to perform over a broad range of steering angles and frequencies. The element patterns at lower frequencies were fairly well behaved over the complete covered range of angles. However, deep nulls (>15 dB) in the element patterns are observed at the four corners along intercardinal cuts, with the angular position of the nulls coming closer to broadside with increasing frequency. These element pattern distortions are expected to limit the off-broadside steering accuracy measurements, especially at higher frequencies.

Fig. 8 shows the array pattern intensity plots as a function of mechanical angle and frequency with the laser wavelengths adjusted for broadside radiation ($\lambda_{az} = 1540$ nm, $\lambda_{el} = 1540.5$ nm). The measured array patterns were normalized by a measured single-element pattern. The azimuth pattern shows the expected performance with the main lobe steered to broadside and narrowing with increasing frequency. The grating lobes may also be observed clearly in these patterns due to the chosen large column separation.

The elevation patterns were measured point-by-point with a fairly large 15° angle increment to keep the measurement time within a reasonable range. Still, the elevation pattern shows the expected broad main lobe, which narrows with increasing frequency but stays steered to broadside. The position of the elevation lobe is shifted to +5° in elevation due to a mechanical boresight misalignment. The elevation lobe is much wider than the azimuth one due to the smaller vertical active element separation.

To demonstrate broad-band squint-free array steering, the laser wavelengths are detuned from the nominal center wavelength to $\lambda_{az} = 1536.4$ nm, $\lambda_{el} = 1536.9$ nm, without any other adjustments. From (1), the array is expected to be steered to −30° in azimuth and −30° in elevation. Fig. 9 shows the measured array pattern intensity plots normalized by a single-element pattern as a function of mechanical angle and frequency. The azimuth pattern clearly shows the main beam lobe steered to −30°. Its positioned is observed to be independent of frequency within the measurement resolution, as expected for true time-delay steering. The grating lobes and two sidelobes are also clearly seen, and show the expected frequency-dependent behavior.

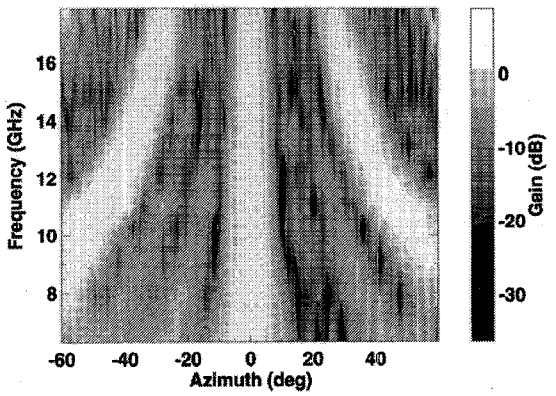

(a)

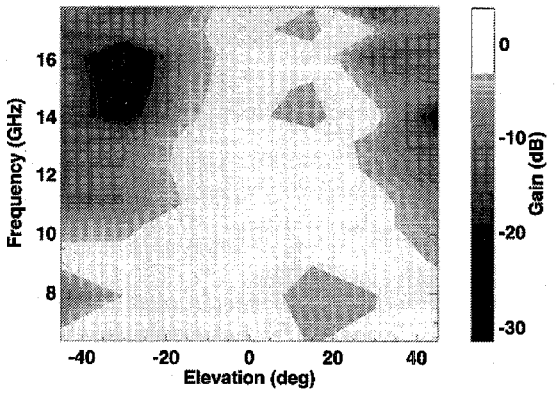

(b)

Fig. 8. Array pattern intensity plots as a function of mechanical angle and frequency with the laser wavelengths adjusted for broadside radiation ($\lambda_{az} = 1540$ nm, $\lambda_{el} = 1540.5$ nm). (a) azimuth scan; (b) elevation scan.

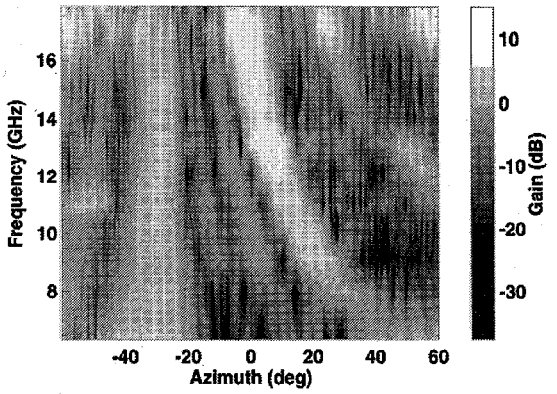

(a)

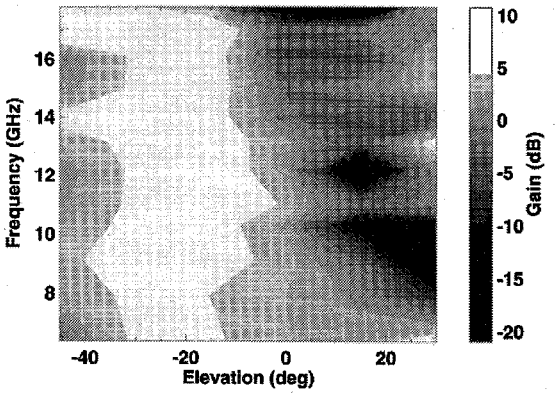

(b)

Fig. 9. Array pattern intensity plots as a function of mechanical angle and frequency with optical steering to $-30°$ azimuth and $-30°$ elevation ($\lambda_{az} = 1536.4$ nm, $\lambda_{el} = 1536.9$ nm). (a) azimuth scan; (b) elevation scan.

The elevation pattern is not as well defined as the azimuth one due to its large measurement angle increment. However, a broad main lobe can be observed at $-25°$ in elevation, with position being frequency independent within measurement resolution. Again, the pattern is shifted from the expected one by $+5°$ due to the boresight misalignment.

Measurements at other azimuth and elevation steering angles are consistent with the results expected for a wideband array transmitter with independent azimuth and elevation time-delay steering over 6–18 GHz.

The wide-band capability and the true time-delay operation of the fiber-optic beamformer can be further illustrated by time-domain characteristics. The available equipment precluded a direct measurement of the system impulse response characteristics. However, the linear time-invariant nature of the system permits an application of a Fourier transform to obtain time-domain characteristics from frequency-domain measurements.

For the sake of clarity of illustration, we have calibrated out the complete system transmission response for the array steered to broadside. This method introduces a caveat in that what is observed is not a true system impulse response, but one corrected for the microwave gain roll off and for the phase deviations from linear with frequency. Thus, the 6 to 18 Ghz frequency measurement range gives a time resolution of 100 ps.

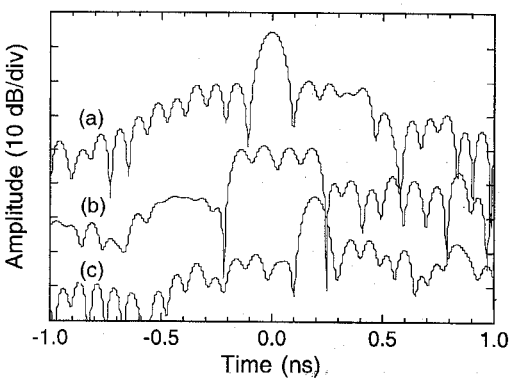

Fig. 10. Time-domain impulse responses calculated from frequency-domain measurements at (a) mechanical and optical broadside; (b) mechanical azimuth of $-60°$ and optical broadside; (c) both mechanical and optical $-60°$ steering.

Fig. 10 shows the time-domain impulse responses calculated from several frequency-domain measurements. The top curve (a) is obtained when the array mechanical and optical steering is set for broadside and exhibits a major transmitted broadband pulse due to the temporal overlap (simultaneous arrival) of all the minor pulses radiating from the individual elements.

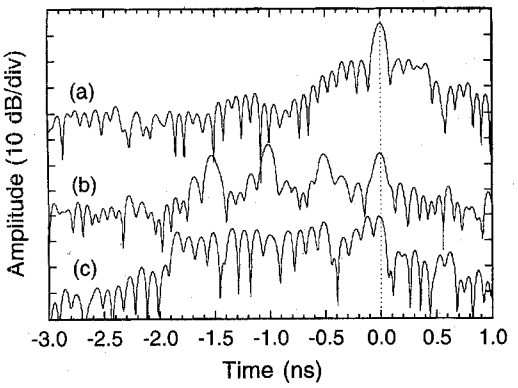

Fig. 11. Time-domain responses calculated from frequency-domain measurements with array steered to mechanical broadside at (a) mechanical and optical broadside; (b) mechanical broadside and optical steering to $\lambda_{az} = 1568$ nm, $\lambda_{el} = 1540.5$ nm; (c) mechanical broadside and optical steering to $\lambda_{az} = 1568$ nm, $\lambda_{el} = 1565$ nm.

When the array is mechanically rotated by $-60°$ in azimuth off broadside while the optical steering is still set for broadside, there is an inherent time-delay introduced into the arrival time to the receiver of the "minor" pulses emitted from column of the elements, and four pulses are clearly resolved [see curve (b)]. These pulses are separated in time proportionally to the column spatial separation. Then, the mechanical angle is left at $-60°$ but the array is steered optically to that same angle by a wavelength detuning of $\Delta\lambda_{az} = -5.9$ nm. All of the emitted pulses are now optically time-delayed such that their arrival time to the receiver is simultaneous, and all pulses overlap temporally again [see curve (c)]. This "major" pulse is time-delayed relative to the broadside case due to the array rotation center not coinciding with the aperture plane and due to one-sided operation of the dispersive time-delay. That is, the one-sided operation cannot delay the arrival time for the elements on one side of the center and advance the arrival time for the other side.

We can also test the limits of the optically-controlled time delay difference that can be introduced in our system. Fig. 11 shows the time-domain responses calculated from frequency-domain measurements with array steered to mechanical broadside. Curve (a) shows the system response with both mechanical and optical steering set for broadside. Curve (b) shows four pulses from the antenna element columns due to the optical delay difference of ~500 ps between columns set by azimuth steering to $\Delta\lambda_{az} = +28$ nm while the elevation is still optically set for broadside ($\Delta\lambda_{el} = 0$ nm). Each one of these pulses can be further separated into a total of 16 pulses due to the individual elements in the column. This is done by introducing a delay difference of ~110 ps between rows via elevation steering to $\Delta\lambda_{el} = +24.5$ nm [see curve (c)].

One of the pulses always stays fixed in time and corresponds to the element fed by fiber-optic links contaning all dispersion-shifted fiber. The amplitude nonuniformity between the pulses may be due to the wavelength dependence of the fiber-optic couplers (see Fig. 6). While these time-delay increments do not correspond to any real array steering angle, they do illustrate the wideband true time-delay operation of the fiber-optic beamformer.

V. Conclusion

We developed a novel fiber-optic true time-delay beamforming technique for broad-band steering of 2-D array antennas. The technique is based on simple dispersive prism optical delay lines, with cascaded prism stages for independent azimuth and elevation steering control. The fiber-optic beamformer was extensively characterized for microwave signal losses, dynamic range, and signal amplitude and phase tracking errors. The performance was consistent with theoretical calculations based on the individual system component characteristics. The fiber-optic beamformer was then used to drive a 4×4 flared-notch transmitter array, and antenna patterns were measured in an anechoic chamber. The measurements show squint-free array steering across a $\pm 30°$ azimuth and $\pm 30°$ elevation range over a 6 to 18 GHz frequency range. We believe this to be a first-ever demonstration of such wideband array steering capabilities in two dimensions.

Acknowledgment

The authors would like to thank J. Valenzi for help with array pattern measurements.

References

[1] I. Frigyes and A. J. Seeds, "Optically generated true-time delay in phased-array antennas," *IEEE Trans. Microwave Theory Tech.*, vol. 43, pp. 2378–2386, Sept. 1995.

[2] J. J. Lee, R. Y. Loo, S. Livingston, V. I. Jones, J. B. Lewis, H. W. Yen, G. L. Tangonan, and M. Wechsberg, "Photonic wideband array antennas," *IEEE Trans. Antennas Propagat.*, vol. 43, pp. 966–982, Sept. 1995.

[3] E. Ackerman, S. Wanuga, D. Kasemset, W. Minford, N. Thorsten, and J. Watson, "Integrated 6-bit photonic true-time-delay unit for lightweight 3–6 Ghz Radar beamformer," in *1992 IEEE MTT-S Dig.*, 1992, pp. 681–684.

[4] N. A. Riza and N. Madamopoulos, "High signal-to-noise ratio birefringence-compensated optical delay line based on a noise-reduction scheme," *Opt. Lett.*, vol. 20, pp. 2351–2353, Nov. 1995.

[5] L. Pang, J. Leonard, T.-H. Lin, G. A. Magel, and S. Eshelman, "Silica-based optical delay lines and switches for phased array radar control," *Proc. SPIE*, vol. 2489, pp. 65–71, 1995.

[6] A. Goutzoulis, K. Davies, J. Zomp, P. Hrycak, and A. Johnson, "A hardware-compressive fiber-optic true time delay steering system for phased-array antennas," *Microwave J.*, pp. 126–140, Sept. 1994.

[7] L. Xu, R. Taylor, and S. R. Forrest, "The use of optically coherent detection techniques for true-time delay phased array and systems," *J. Lightwave Technol.*, vol. 13, pp. 1663–1678, Aug. 1995.

[8] E. N. Toughlian, H. Zmuda, and P. Kornreich, "A deformable mirror-based optical beamforming system for phased array antennas," *IEEE Photon. Technol. Lett.*, vol. 2, pp. 444–446, June 1990.

[9] G. A. Ball, W. H. Glenn, and W. W. Morey, "programmable fiber optic delay line," *IEEE Photon. Technol. Lett.*, vol. 6, pp. 741–743, June 1994.

[10] S. T. Johns, D. A. Norton, C. W. Keefer, R. Erdmann, and R. A. Soref, "Variable time delay of microwave signals using high dispersion fiber," *Electron. Lett.*, vol. 29, pp. 555–556, Mar. 1993.

[11] M. Y. Frankel and R. D. Esman, "True time-delay fiber-optic control of an ultrawideband array transmitter/receiver with multibeam capability," *IEEE Trans. Microwave Theory Technol.*, vol. 43, pp. 2387–2394, Sept. 1995.

[12] D. G. Cooper, J. L. Dexter, and R. D. Esman, "Widely tunable polarization-stable fiber lasers," *IEEE J. Select. Topics Quantum Electron.*, vol. 1, pp. 14–21, Apr. 1995.

[13] B. H. Kolner and D. W. Dolfi, "Intermodulation distortion and compression in an integrated electrooptic modulator," *Appl. Opt.*, vol. 26, pp. 3676–3680, Sept. 1987.

[14] Hughes Ground Systems Group, El Segundo, CA, vol. 37, no. 9.

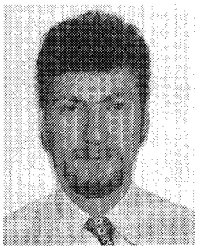

Michael Y. Frankel was born in St. Petersburg, Russia, in 1964. He received the B.S. degree (*magna cum laude*) from the University of Maryland, College Park, in 1986, the M.S. degree from the University of Rochester in 1988, and the Ph.D. degree from the University of Michigan, Ann Arbor, in 1991, all in electrical engineering.

He is currently with the Optical Sciences Division, Naval Research Laboratory. He is actively involved in developing lasers and modulators for fiber-optic microwave links. He is also pursuing novel photonic beamforming techniques for phase-array antennas. His other interests are in ultrafast optoelectronic studies and modeling of semiconductor materials, high-speed transmission lines, photodetectors, and transistors.

Dr. Frankel has over 50 publications and conference presentations in these areas and several patents.

Paul J. Matthews received the B.S. degree (*magna cum laude*) in physics from Loyola University of Chicago, IL, in 1986, and the M.S. and Ph.D. degrees in electrical engineering from the University of Colorado, Boulder, in 1988 and 1991, respectively.

His Ph.D. dissertation centered on the fabrication and characterization of LiNbO3 and LiTaO3 integrated optical devices for microwave applications. From January 1992 to October 1992, he was employed by CAI/Recon Optical. In October 1992 he joined the staff of the Advanced Photon Source at Argonne National Laboratory where he was engaged in efforts to design, model and fabricate a mm-wave linear accelerator using deep-etch X-ray lithography techniques and electroplating. Since September 1995, he has been with the Optical Sciences Division of the Naval Research Laboratory where he is currently investigating optical control schemes for phased array radar applications.

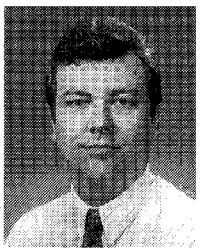

Ronald D. Esman (S'82–M'85–SM'95) received the B.A. degree (*magna cum laude*) in physics and mathematics from Kalamazoo College, Kalamazoo, MI, in 1981. In 1980, he interned at Oak Ridge National Laboratory, Oak Ridge, TN, where his research included characterization and passivation of polycrystalline Si solar cells. He received the M.S. and D.Sc. degrees in electrical engineering from Washington University, St. Louis, MO, in 1983 and 1986, respectively.

His doctoral thesis research was in the areas of fabrication, large-signal analysis, and characterization of high-speed electroabsorption avalanche photodetectors. He joined Naval Research Laboratory, Washington, DC, in 1986, where he began work in the fields of high-speed optoelectronics, optical-microwave interactions, semiconductor laser noise and spectral characteristics, and fiber optics. He was with NIST, Boulder, CO, from 1990 to 1991, where he studied high-speed coherent optical transmission and measurement techniques at NTT Transmission Systems Laboratory, Yokosuka, Japan. He is presently Head of the Fiber-Optic Microwave Signal Processing Section at NRL, which is involved in RF array beamforming, remote sensing, photodetector nonlinearities, and picosecond optical probing.

Dr. Esman is a member of Sigma Xi and the Optical Society of America.